Enhanced in and out-coupling of InGaAs slab waveguides by periodic metal slit arrays

Seung Hyun Kim,[1,2] Chung Min Lee,[1] Seung Bo Sim,[3] Jin hee Kim,[3] Jang hee Choi,[1,4] Won Seok Han,[4] Kwang Jun Ahn,[5,6] and Ki Ju Yee[1,2,*]

[1]*Department of Physics, Chungnam National University, Daejeon 305-764, Korea*
[2]*GRAST, Chungnam National University, Daejeon 305-764, Korea*
[3]*Korea Research Institute of Standards and Science, Daejeon 305-340, Korea*
[4]*Electronics and Telecommunications Research Institute, Daejeon 305-700, Korea*
[5]*Center for Subwavelength Optics and Department of Physics and Astronomy, Seoul National University, Seoul 151-747, Korea*
[6]*kwangjun@phya.snu.ac.kr*
[*]*kyee@cnu.ac.kr*

Abstract: We studied the in- and the out-coupling efficiencies of photons with a thin InGaAs slab covered by periodic gold nano-slit arrays, by measuring transmission and photoluminescence (PL) spectra. While the maximum in-coupled photons into the InGaAs slab waveguide were found at dip positions in transmission spectra, the mostly out-coupled photons were observed as peaks in PL spectra. For different periods of slit arrays and incident angles we discussed spectral positions of transmission dips and efficiency of the in-coupling influenced by the absorption coefficient of InGaAs. In PL spectra we measured overall enhanced PL intensities from the InGaAs slab covered by slit arrays compared to that of a bare InGaAs, where the peak positions are determined by the period of slit arrays as well. Our findings are important for designing semiconductors both as an optically passive waveguide and active light emitter.

OCIS codes: (050.6624) Subwavelength structures; (230.7400) Waveguides, slab.

References and links

1. R. E. Collin, *Field Theory of Guided Waves*, 2nd ed, D. G. Dudley ed (Wiley-IEEE Press., New York, 1991).
2. R. G. Harrington, *Time-Harmonic Electromagnetic Fields*, D. G. Dudley ed. (John Wiley & Sons Inc., New York, 2001).
3. S. Y. Lin, E. Chow, V. Hietala, P. R. Villeneuve, and J. D. Joannopoulos, "Experimental demonstration of guiding and bending of electromagnetic waves in a photonic crystal," Science **282**(5387), 274–276 (1998).
4. T. W. Ebbesen, H. J. Lezec, H. F. Ghaemi, T. Thio, and P. A. Wolff, "Extraordinary optical transmission through sub-wavelength hole array," Nature **391**(6668), 667–669 (1998).
5. F. J. Garcia-Vidal and L. Martin-Moreno, "Transmission and focusing of light in one-dimensional periodically nanostructured metals," Phys. Rev. B **66**(15), 155412 (2002).
6. R. W. Wood, "Anomalous Diffraction Gratings," Phys. Rev. **48**(12), 928–936 (1935).
7. H. Raether, *Surface Plasmons on Smooth and Rough Surfaces and on Gratings,* G. Hohler ed. (Springer-Verlag, Berlin 1998).
8. H. Lochbihler and R. Depine, "Highly conducting wire gratings in the resonance region," Appl. Opt. **32**(19), 3459–3465 (1993).
9. M. S. Shishodia and A. G. Unil Perera, "Heterojunction plasmonic midinfrared detectors," J. Appl. Phys. **109**(4), 043108 (2011).
10. A. D. Rakic, A. B. Djurisic, J. M. Elazar, and M. L. Majewski, "Optical properties of metallic films for vertical-cavity optoelectronic devices," Appl. Opt. **37**(22), 5271–5283 (1998).
11. S. Adachi, *Physical Properties of III–V Semiconductor Compounds* (John Wiley & Sons, Inc., New York, 1992).
12. K. G. Lee and Q.-H. Park, "Coupling of surface Plasmon polaritons and light in metallic nanoslits," Phys. Rev. Lett. **95**, 103902 (2005).
13. X. Zhang, B. Sun, J. M. Hodgkiss, and R. H. Friend, "Tunable ultrafast optical switching via waveguided gold nanowires," Adv. Mater. (Deerfield Beach Fla.) **20**(23), 4455–4459 (2008).
14. D. de Ceglia, M. A. Vincenti, M. Scalora, N. Akozbek, and M. J. Bloemer, "Plasmonic band edge effects on the transmission properties of metal gratings," AIP Advances **1**(3), 032151 (2011).
15. N. Finger, W. Schrenk, and E. Gornik, "Analysis of TM-Polarized DFB laser structures with metal surface gratings," IEEE J. Quantum Electron. **36**(7), 780–786 (2000).

#160017 - $15.00 USD Received 19 Jan 2012; revised 18 Feb 2012; accepted 26 Feb 2012; published 5 Mar 2012

16. B. R. Bennett, R. A. Soref, and J. A. Del Alamo, "Carrier-induced change in refractive index of InP, GaAs, and InGaAsP," IEEE J. Quantum Electron. **26**(1), 113–122 (1990).
17. T. Gong, W. L. Nighan, and P. M. Fauchet, "Hotcarrier Coulomb effects in GaAs investigated by femtosecond spectroscopy around the band edge," Appl. Phys. Lett. **57**(25), 2713–2715 (1990).
18. J. Hader, S. W. Koch, and J. V. Moloney, "Microscopic theory of gain and spontaneous emission in GaInNAs laser material," Solid-State Electron. **47**(3), 513–521 (2003).

1. Introduction

Waveguides are optical systems via which photons are transferred from one position to another. Propagation properties of photons in waveguides are determined by geometry and materials forming the waveguide. The cutoff wavelength, eigenmodes, and propagation losses of diverse waveguides have intensively been studied [1, 2]. In special, dielectric waveguides are mostly preferred for photons in wide frequency range from visible to far-infrared. Based on the total internal reflection appearing when photons in an optically dense medium propagate into a lower one, dielectric waveguides are basically composed of two dielectrics with high refractive index contrast, the higher refractive index material as the core and the lower one for the cladding. Besides the propagation characteristics of guided photons, other critical properties are the in- and the out-coupling of photons into/from the waveguides, especially when their cross sections approach the diffraction limit.

Compared to optically passive dielectric waveguides, semiconductor waveguides have advantage in that their optical properties can be controlled by electrical or optical means [3]. In addition, they can simultaneously perform as gain media and waveguides as found in semiconductor lasers. However, when the dimensions of semiconductor waveguides are decreased, they confront the same problems discussed above, the reduction of the in- and the out-coupling of photons. Furthermore, more careful consideration is required for semiconductor waveguides due to strongly dispersive behaviors of the refractive index and the absorption coefficient near the semiconductor band gap.

Since extraordinary transmission of electromagnetic wave was demonstrated through two-dimensional hole arrays perforated at thin metals [4], surface plasmon polaritons (SPP) are attracting great interests not only academically but also for applications. Surface plasmon is a guided mode propagating along the metal-dielectric interface. In one dimensional slits [5] or two dimensional holes [6], there exist wavelengths where strongly surface-confined modes can be induced by photons, known as surface plasmon excitation [7]. One promising way for enhanced coupling of photons with materials is to combine periodic sub-wavelength structures with them.

In this paper, we report on enhanced coupling of photons into and from semiconductor waveguide structure via an additional momentum supported by one dimensional metallic slit array. We measured transmission and photoluminescence (PL) spectra of an InGaAs slab waveguide covered by different periods of gold nano-slit arrays. Additionally, theoretically obtained transmission spectra which are in good agreement with experiment were presented. We discussed the in- and the out-coupling of the InGaAs slab waveguide, which are related to magnitudes and spectral positions of transmission dips and PL peaks, respectively.

2. Experimental and theoretical methods

An $In_{0.53}Ga_{0.47}As$ layer with a thickness of 370 nm was grown on an InP substrate by metal-organic chemical vapor deposition (MOCVD) technique. An Au layer with a thickness of 50 nm was deposited upon it, with an insertion layer of 3 nm-thick Ti for stronger adhesion of the metal on the InGaAs layer. One dimensional slit arrays were fabricated in the Au layer using e-beam lithography technique, where the period of slit arrays was varied from 390 nm to 500 nm while the opening ratio (aperture length to period) was maintained at 40%. Each pattern has a dimension of 50 μm x 100 μm where the short dimension is the length of slits. A SEM image of fabricated metal grating with a period of 420 nm is shown in inset of Fig. 1(b).

Transmission and PL spectra were measured for each pattern at room temperature. A super-continuum light source was focused onto each pattern for measuring transmission spectra. The spot size at metal slits was about 30 μm, illuminating about 70 slits in the focal

#160017 - $15.00 USD Received 19 Jan 2012; revised 18 Feb 2012; accepted 26 Feb 2012; published 5 Mar 2012

spot. The angle of the incident beam was estimated to be dispersed within +/−2°, as it was calculated from the incident beam diameter and focal length. The incident wave was transversal magnetic (TM) polarized perpendicular to the slit axis as illustrated in Fig. 1(a), and transmitted field intensity was measured by a monochromator and an InGaAs photodiode in the near-infrared (IR) wavelength regime. For PL measurement, each pattern was excited by a Ti:sapphire laser with a wavelength of 800 nm and the luminescence was collected at front of metal slits.

In order to compare experimental results with theory, transmission spectrum was calculated by using a modal expansion model with surface impedance boundary condition (SIBC) matching. Compared to the previous model of Lochbihler *et al.* [8], we included additional thin InGaAs layer between the metal slit layer and the half-infinite InP substrate (Fig. 1(a)). For the TM field excitation from air, the magnetic field in the thin layer has the y-component only, which is written as

$$H_y(x,z) = \sum_n A_n \exp(i(k_{xn}x + k_{zn}z)) + B_n \exp(i(k_{xn}x - k_{zn}z)), \quad (1)$$

where A_n and B_n are the reflection coefficients at the InGaAs-InP and the InGaAs-air interface, respectively, k_{xn} is the transversal wave number at an order of n, and k_{zn} the corresponding wave number in the z-direction. k_{zn} depends on the dielectric constant of InGaAs ε_{InGaAs} and the wavelength $\lambda = 2\pi/k_0$ of the incident field through the relation $k_{zn} = \sqrt{\varepsilon_{InGaAs} k_0^2 - k_{xn}^2}$.

The transmittance coefficient t_n through the InP substrate region was derived by fulfilling the continuity of transversal field components at each interface and SIBC matching at metal-dielectric interfaces. For the transmission spectrum we calculated Poynting vector ($\propto \mathrm{Re}[\boldsymbol{E} \times \boldsymbol{H}^*]$) in the far-field. Recently, a metal slit array on a GaAs/AlGaAs/GaAs structure was theoretically studied for plasmonic mid-IR detectors, for which a similar theoretical model was presented [9]. In numerical calculations we used frequency-dependent complex permittivity for gold [10] and $In_{0.53}Ga_{0.47}As$ [11], respectively. A constant dielectric constant was used for InP. For each slit period we calculated the dispersion relations up to the 3rd order, but there were no qualitative difference in transmission spectra from those considered only the 0th order.

#160017 - $15.00 USD Received 19 Jan 2012; revised 18 Feb 2012; accepted 26 Feb 2012; published 5 Mar 2012

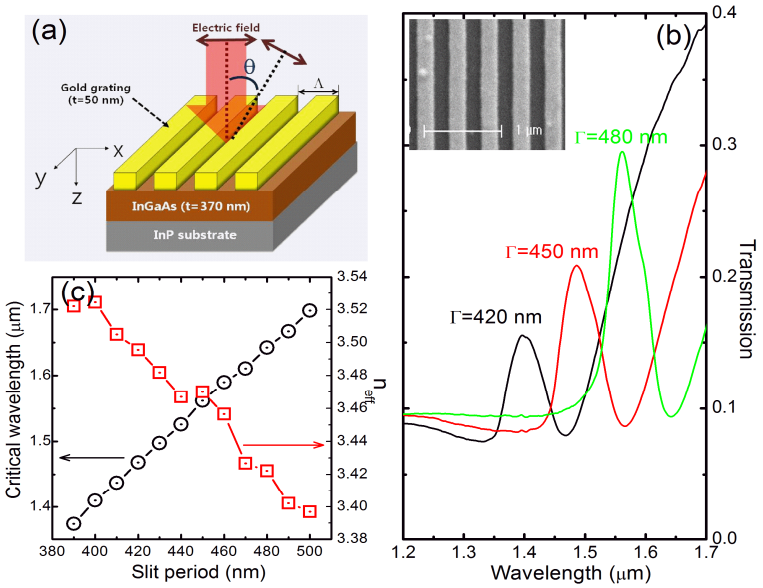

Fig. 1. (a) Schematic of the InGaAs slab waveguide structure covered by periodic gold nano-slit array. The thickness of InGaAs and gold is 370 nm and 50 nm, respectively. The opening ratio is 40% in each metal grating. Electric field of the incident light was TM polarized and the incident angle θ was changed in the transmission measurement. (b) Transmission spectra measured for metal slits with different periods at normal incidence. Inset is a SEM image for the slit with a period of 420 nm. (c) Critical wavelength with a dip in transmission spectra and the corresponding effective refractive index (n_{eff}) as a function of slit period.

3. Results and discussion

Figure 1(b) shows the transmission spectra of our samples with the grating period of 420 nm, 450 nm, and 480 nm for normal incidence. All in all, they show a similar spectral shape as observed in other wavelength regimes [12–14]. The transmission shows increasing behavior as the wavelength increases beyond the band gap of $In_{0.53}Ga_{0.47}As$ about $\lambda \approx 1650$ nm at room temperature [11]. However, for each grating pattern there is a wavelength region where the transmission modulates strongly. The transmission of the period $\Lambda = 480$ nm, for an instance, increases from 10% to 30% and then drops to 10% at around 1.6 μm. We interpret the drastic transmission change at the spectral dip as occurring by the resonant excitation of surface plasmons at the interface of the gold and the InGaAs waveguide. Since the thickness of InGaAs layer, in this case, is rather small, the nature of the surface plasmon mode is influenced by the coexistence of the InGaAs and InP. The slit period determines transversal wave vector k_x of the resonant surface plasmon mode at normal incidence, and the effective refractive index n_{eff}, which is defined as the value of the wavelength divided by the slit period such that $n_{eff} = \lambda / \Lambda$, accounting for the in-plane propagation speed of the mode.

In Fig. 1(c) the dip position (black circles) and the effective refractive index of the corresponding mode (red squares) are presented as a function of the slit period. With increasing the period, the effective refractive index decreases generally. The measured effective refractive index of corresponding mode having a value between 3.38 and 3.52, is smaller than the refractive index of bulk $In_{0.53}Ga_{0.47}As$ layer, which is around 3.6 from Adachi's model [11]. We note that the small n_{eff} value of the transmission dip may have resulted from the substantial intrusions of the electromagnetic field into air as well as the InP substrate region. The tendency of the effective refractive index depending on the slit period results also from the embedment of the InGaAs thin layer between the metal and the substrate. We numerically confirmed (not shown here) that the effective refractive index of same slit

#160017 - $15.00 USD Received 19 Jan 2012; revised 18 Feb 2012; accepted 26 Feb 2012; published 5 Mar 2012

arrays attached directly on a half-infinite substrate is exactly the same value of the substrate and does not change for varying the slit period. We should note that the resonance wavelengths of SPP [7] at the interface of gold and semi-infinite InGaAs layer lie larger than the position of the transmission dip. For an example, the slit array with a period Λ = 450 nm has the resonance at a wavelength of 1.65 μm determined by $\lambda_{spp} = \Lambda \times \sqrt{\varepsilon_{InGaAs}\varepsilon_{Au} / (\varepsilon_{InGaAs} + \varepsilon_{Au})}$, where a constant dielectric constant of InGaAs ε_{InGaAs} = $3.6^2 \approx 13.0$ was assumed.

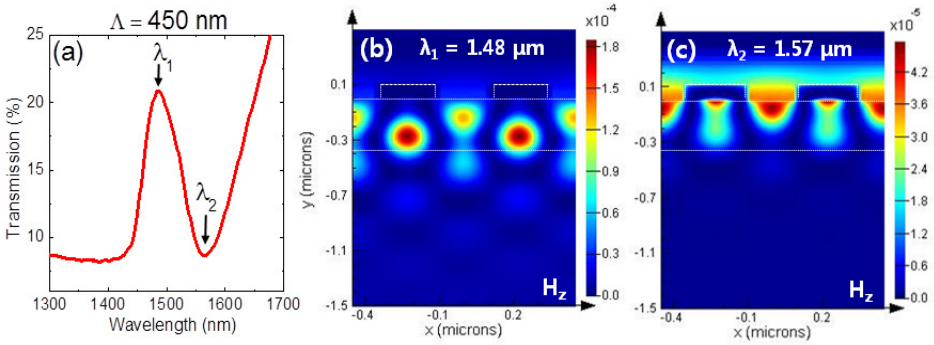

Fig. 2. (a) Transmission spectrum measured for metal slit array with Λ = 450 nm at normal incidence. The arrows indicate positions of transmission peak and dip at 1,480 nm and 1,570 nm, respectively. Spatial distribution of H_z field obtained from FDTD simulation at the same condition with the measurement is shown for the transmission peak (b), and for the transmission dip (c) wavelength.

To verify origin of the peak and the dip in transmission spectrum, we have performed FDTD (finite-difference time domain) simulation for the same conditions with transmission measurements. The arrows at λ_1 = 1,480 nm and λ_2 = 1,570 nm in Fig. 2(a) indicate the positions of transmission peak and dip, respectively, for a metal slit array with Λ = 450 nm. The FDTD results of spatial H_z field distributions were presented in Fig. 2(b) for the transmission peak and in Fig. 2(c) for the dip. At the transmission peak (Fig. 2(a)), large portion of the incident field transfers to the InP substrate layer through the subwavelenth gold slit array. On the other hand, the H_z field is strongly confined around the interface of InGaAs and the Au slit array at the dip (Fig. 2(c)). Thus, the FDTD simulation supports that the transmission dip originates from the resonant excitation of surface plasmonic guided modes. For the resonant surface plasmon mode, it is evident from Fig. 2(c) that strong field distribution at air aperture between metal slits would shift the resonance wavelength deviating from the case of flat metal without slits [14].

#160017 - $15.00 USD Received 19 Jan 2012; revised 18 Feb 2012; accepted 26 Feb 2012; published 5 Mar 2012

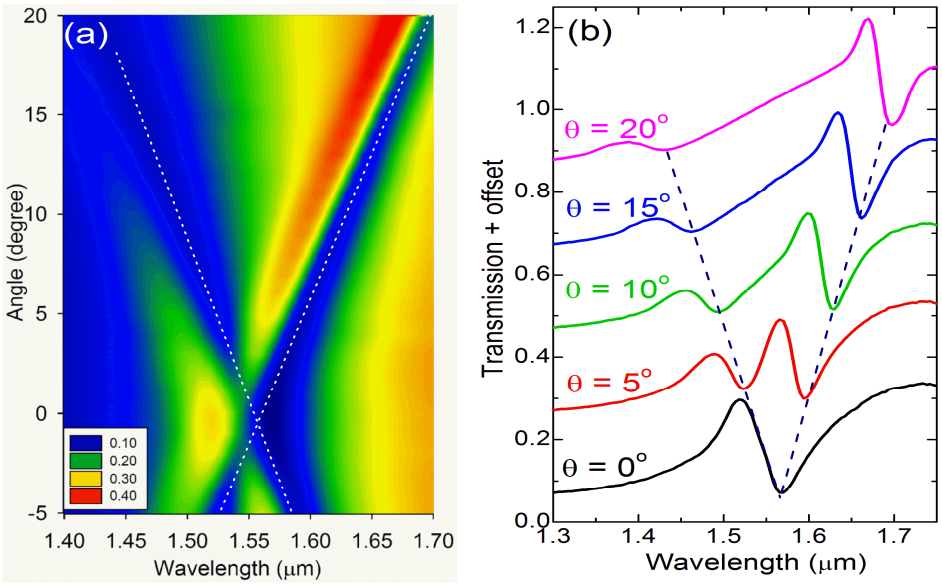

Fig. 3. (a) Contour plot of the measured transmission spectrum with the wavelength as horizontal axis and the incident angle as vertical axis. (b) Transmission spectra measured at different incident angles for the slit array with a period of 470 nm. The dashed lines show the evolution of the transmission dip with an incident angle

Our sample structure, high-index dielectric (InGaAs) as the core and metal and low-index dielectric (InP) as the cladding, sustains guiding modes along the x-direction. The waveguide supports only one TE and one TM mode when the perforated metallic slits are replaced by a flat metal film. At shorter wavelength region of transmission peak, at around 1.33 μm for the case of Λ = 420 nm, one can notice another broad transmission minimum, which might originate from the excitation of conventional TM guided mode.

In our surface corrugated waveguide structure, the guiding modes with multiples of the grating momentum ($k_w = 2\pi m/\Lambda$, m = $\pm$ 1, $\pm$ 2, …) can resonantly be excited if the frequency of the normal incident photon matches the guided mode. The resonant excitation of the modes will appear as a dip in the far-field transmission spectrum. If the incident light is inclined with an angle θ from the surface normal as depicted in Fig. 1(a), the guiding modes will have an additional momentum. The momentum conservation forces to $k_w = k_0 \sin\theta \pm mK_G$, where $K_G = 2\pi m/\Lambda$ is the grating momentum.

Figure 3(a) shows contour plot of the measured transmission as a function of the wavelength and the incident angle for a grating period of 470 nm. As the incident angle increases, the degeneracy of the guiding mode at the normal incidence is removed so that two transmission dips appear. In Fig. 3(b) we depicted representatively line profiles at a few selected incident angles. Two spectral dips supporting the surface plasmon modes are clearly seen. The high energy mode with the shorter wavelength corresponds to the mode propagating in the same direction of the incident photon projected on the waveguide axis while the low energy mode with the longer wavelength propagates in the opposite direction.

#160017 - $15.00 USD Received 19 Jan 2012; revised 18 Feb 2012; accepted 26 Feb 2012; published 5 Mar 2012

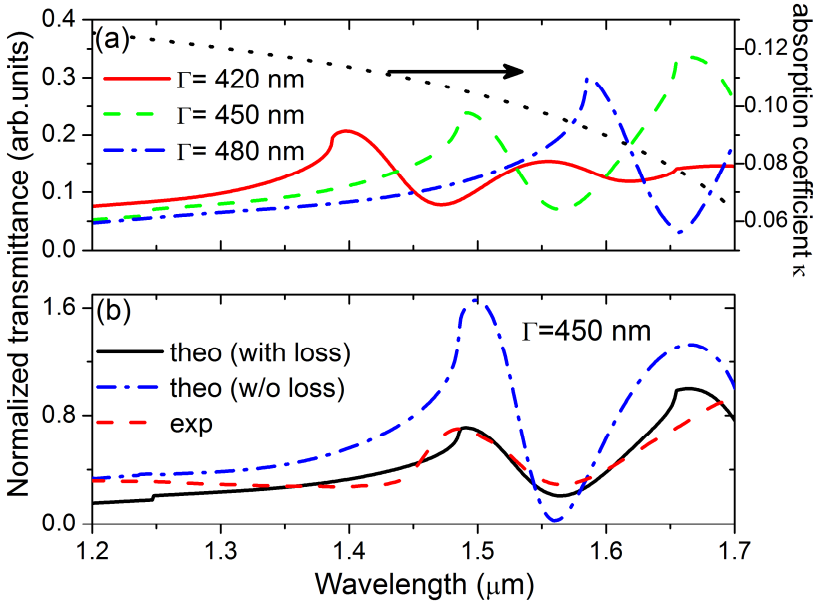

Fig. 4. (a) Calculated transmission spectra using a modal expansion model for grating period of 420, 450, and 480 nm. Dotted line is the absorption coefficient dispersion of the InGaAs material used in the simulation. (b) Comparison of the experimental and theoretical transmission spectrum for a grating with Λ = 450 nm. The transmittance for the same condition but without absorption (Im[ε_{InGaAs}] = 0) is shown together.

In Fig. 1(b) and Fig. 3(a) we can find two consistent trends that *i)* the transmission modulation (the ratio between the peak and the dip value of the transmittance) is stronger when the peak and the dip positions are located at longer wavelengths and *ii)* the transmittances at all dip positions are not completely null, meaning that there are leakage waves from guided waves in the InGaAs layer. We estimate that these behaviors are attributed to the dispersive absorption coefficient of the InGaAs material, depicted as a dotted line in Fig. 4(a). In order to investigate the in-coupling properties of our waveguide structure, we calculated the transmittance and compared results to measurements. In Fig. 4(a) the transmittances of three different periods (Λ = 420 nm, 450 nm, and 480 nm) are presented. There are slight differences between theory and experiment in the spectral shape, where the wavelength of the transmission dip shifts according to refractive indices used for the InGaAs and the InP layer. For a quantitative comparison we plotted the calculated and measured transmittance of the Λ = 450 nm sample in Fig. 4(b), where the non-vanishing transmittances at the dip position is well reproduced by our theoretical model. We also represented the transmittance for the same condition but without absorption (Im[ε_{InGaAs}] = 0). While the peak and the dip position do not change, the transmission modulation increases and the transmittance at the dip position is almost null. Therefore, the absorption coefficient of the waveguide core material influences not only the propagation of guided waves but in-coupling of the incident wave as well.

Next, we studied the out-coupling efficiency of our surface-corrugated waveguide from the InGaAs region to radiation field into air. For this purpose we generated the PL signal at the InGaAs layer by optically pumping electrons above the band gap. PL spectrum measured from a bare InGaAs layer at room temperature is shown as the dashed line in Fig. 5(a) and shows a broad peak around 1560 nm with a FWHM (full-width at half-maximum) of 200 nm. PL spectra of samples covered by metal gratings with different periods (Λ = 410 nm, 440 nm, 470 nm, and 500 nm) are presented in Fig. 5(a) as well. The shapes of the PL spectra deviate substantially from that of the bare InGaAs. The wavelength at the maximum PL intensity depends linearly on the grating period as plotted in inset of Fig. 5(a). The maximum PL

#160017 - $15.00 USD Received 19 Jan 2012; revised 18 Feb 2012; accepted 26 Feb 2012; published 5 Mar 2012

intensity of the Λ = 470 nm sample shows almost a four-fold enhancement compared to the PL of the bare InGaAs at the same wavelength.

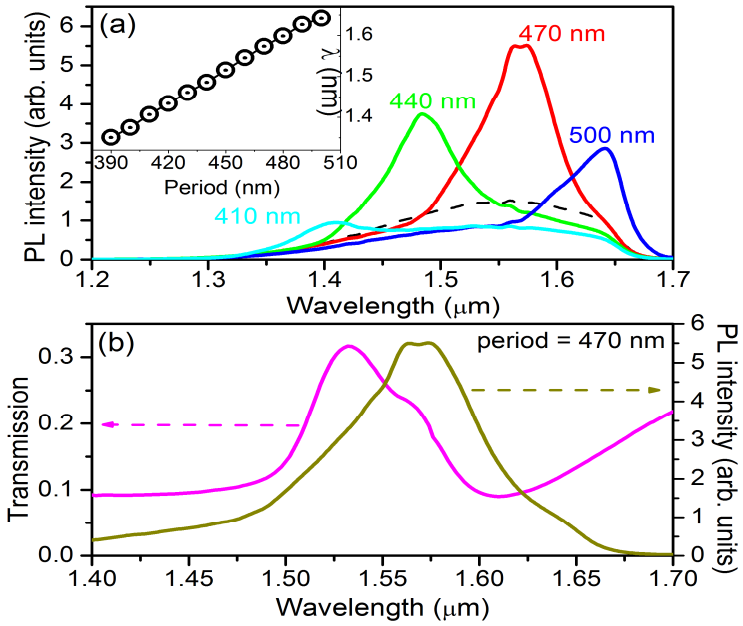

Fig. 5. (a) PL spectra measured for slit arrays with different periods. The dashed line is PL signal from the bare InGaAs without metal grating. Inset is wavelength of the maximum PL enhancement as a function of grating period. (b) Comparison of PL and transmission spectrum for the same slit period of 470 nm.

When the InGaAs layer changes to optically active medium emitting photons, the sample structure is similar to a distributed feedback (DFB) semiconductor laser with metal surface gratings [15]. The Bragg condition of DFB lasers is given by $\Lambda = N\lambda/2n_{eff}$ where N is the coupling order. In the first order (N = 1), photons at the one end of the period in the waveguide are positively interfered by the photons reflected from the other end because both photons are in a same phase. Thus, amplified photons are emitted from both edges of the structure. In the second order (N = 2) the guided photons are partially transformed into propagating photons in ± z direction, i.e. the surface-emitting mode of light [15]. Note that the second order Bragg condition is exactly same as the resonant SPP excitation condition in the transmission. Thus, for a slit period Λ the spectral dip in the transmission spectrum and the peak in PL spectrum are expected to be located at a same spectral position. In Fig. 5(b) we displayed the transmission (red solid line) and the PL spectrum (blue dashed lines) of a Λ = 470 nm pattern. For an easy comparison we normalized both spectra with each maximum value. While the spectral dip in the transmission spectrum is found at λ≈1.61 μm, the peak in the PL spectrum is approximately located at λ≈1.58 μm. The effective refractive indices given by dividing above wavelengths with the slit period are obtained as 3.43 for the transmission dip and 3.35 for the PL peak. We checked other periods of samples and found the smallest and the largest refractive index change $\Delta n_{min} = 0.06$ for a Λ = 390 nm and $\Delta n_{max} = 0.11$ for a Λ = 500 nm sample.

It is well known that free charge carriers induce a refractive index change [11, 16]. We calculated the wavelength-dependent refractive index change Δn(λ) by using the following equation:

$$\Delta n(\lambda) = -\frac{e_0^2\lambda^2}{8\pi^2 n(\lambda)\varepsilon_0 c_0^2}\left(\frac{N_e}{m_e} + N_p\frac{m_{lh}^{1/2}+m_{hh}^{1/2}}{m_{lh}^{3/2}+m_{hh}^{3/2}}\right), \quad (2)$$

#160017 - $15.00 USD Received 19 Jan 2012; revised 18 Feb 2012; accepted 26 Feb 2012; published 5 Mar 2012

where e_0 is elementary charge, ε_0 vacuum permittivity, c_0 speed of light, N_e (N_p) free electron (hole) density, and m_e, m_{lh}, and m_{hh} are effective electron, light hole, and heavy hole mass of $In_{0.53}Ga_{0.47}As$, respectively. Since our $In_{0.53}Ga_{0.47}As$ layer was not doped, we used the same value for N_e and N_p which was estimated from optical pump power (N_e~10^{18}/cm^3). We numerically observed the same tendency of the refractive index change, but the value was rather smaller than the measured value of 0.1. The reason might be the carrier-carrier scattering [17, 18] or the stimulated emission processes which can change the photoluminescence spectra.

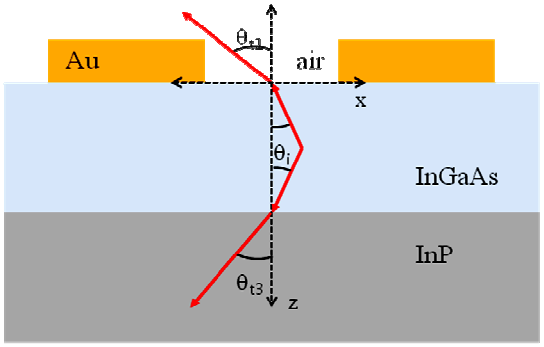

Fig. 6. Schematic illustration of transmittance of photons emitted from InGaAs layer into air and InP substrate. θ_i denotes the incident angle and θ_{t1} and θ_{t3} are the transmission angles in air and InP, respectively.

To ascertain the four-fold PL enhancement of the metal slit-covered layer compared to that of the bare film, in Fig. 6, we schematically illustrate the wave diffractions at both interfaces. At the InGaAs-InP interface the total internal reflection angle θ_t is not influenced by the metallic slit layer and approximately given as 63.1 degrees for n_{InP} = 3.2 and n_{InGaAs} = 3.6. At the air-InGaAs interface the total internal reflection angle is given as 15.7 degrees for the bare case. Only 2% of photons generated in the InGaAs layer escape the bare InGaAs layer. The other photons are reflected back at the interface and contribute to the waveguide modes, propagating along the InGaAs layer. On the contrary, due to the grating momentum for the slit-covered case, the total internal reflection angle is changed to a wavelength-dependent function:

$$\theta_i = \sin^{-1}\left(\frac{n_{air}}{n_{InGaAs}} \pm \frac{N\lambda}{n_{InGaAs}\Lambda}\right). \qquad (3)$$

We find easily that the value in the parenthesis for the upper case (+) is always larger than 1 in our considered wavelengths and slit periods. In the lower case (-) for the first order diffraction, the total internal reflection angle varies in 29.5 ° ≤ θ_t ≤ 65 ° for Λ = 390 nm and 18.9 ° ≤ θ_t ≤ 40 ° for Λ = 500 nm in the wavelength range 1.1 μm ≤ λ ≤ 1.7 μm. The photons escaping the waveguide are substantially increased due to the efficient out-coupling of the guided photons, caused by the additional grating momentum. Therefore, the PL intensity can be enhanced by the existence of the metallic grating, instead of being blocked by the metal layer.

5. Conclusion

We studied the in- and the out-coupling efficiency of photons with an InGaAs slab structure covered by 1D gold nano-slit array. Additional grating momentum supported by periodic slits enabled efficient coupling of the incident photons into/from the guided mode, which were observed as a dip in transmission and a peak in PL spectrum. By comparing experiment with theory we found that non-negligible absorption coefficient of InGaAs waveguides gave rise to weakened in-coupling efficiencies of photons into guided modes. The enhanced out-coupling

#160017 - $15.00 USD Received 19 Jan 2012; revised 18 Feb 2012; accepted 26 Feb 2012; published 5 Mar 2012

efficiencies of photons from waveguides were revealed by PL experiments where substantially enhanced PL intensities were observed for InGaAs covered by slit arrays, and explained by increased total reflection angles at the InGaAs-air interface due to additional grating momentums of slit arrays.

Acknowledgments

This work was supported by the National Research Foundation of Korea Grants funded by the Korean Government (Basic Science Research Program: 2009-0085432, 2009 University-Institute cooperation program, SRC: 2010-0001859).

#160017 - $15.00 USD Received 19 Jan 2012; revised 18 Feb 2012; accepted 26 Feb 2012; published 5 Mar 2012